J Solid State Electrochem (2006) 10: 223–229
DOI 10.1007/s10008-005-0670-x

ORIGINAL PAPER

M. Bouroushian · T. Kosanovic

Electrochemical formation and composition analysis of $Zn_xCd_{1-x}Se$ solid solutions

Received: 28 September 2004 / Revised: 19 October 2004 / Accepted: 7 March 2005 / Published online: 10 June 2005

Abstract The direct growth of ZnSe–CdSe solid solution onto metallic cathodes by electrodeposition from acidic aqueous sulphate solutions is described. The plating process is studied by simple voltammetry, while the structure and composition of the electrolytic deposits are investigated by X-ray diffraction. The experimental *d*-spacing values of the as-grown mixed lattice are compared to data from reference $Zn_xCd_{1-x}Se$ pellets of standard composition, produced by a sintering method. The findings are supplemented with energy-dispersive X-ray (EDX) elemental analysis. Thereupon, the variation of the mole fraction x in $Zn_xCd_{1-x}Se$, and the solid phase constitution of the electrodeposits are determined and correlated to the electrochemical conditions of growth. The resulting films contain admixtures of CdSe compound and metallic Cd.

Keywords Zinc–cadmium-selenide · Electrodeposition · X-ray diffraction · Solid solutions

Introduction

The solid solutions of binary II–VI semiconductive compounds present a great capability for various applications mainly in optoelectronics, as their properties can be engineered with respect to the atomic composition. Specifically, the $Zn_xCd_{1-x}Se$ (ZCS) alloy in thin film form is of considerable interest for the development of tandem solar cells as well as for the fabrication of superlattices and phosphor materials for monitors [1–8]. ZCS is a combination of the CdSe and ZnSe binary direct-gap semiconductors. As the band gap energies of these compounds differ significantly (1.7 and 2.7 eV, respectively), the electronic properties of the alloy can be systematically varied by an appropriate choice of the mole fraction (x) within the energetic range defined by the end members—though rather not in a linear manner [2, 9].

Cadmium selenide was investigated thoroughly during the last decades and has found applications in the field of photo-catalysis and conversion of solar energy, particularly in photoelectrochemistry due to the possibility of stabilization against photocorrosion [10, 11]. On the other hand, zinc selenide and the ZnSe-based materials are now the most promising candidates of light emitting and laser diode devices in the blue–green spectral region [6, 12, 13]. In the CdSe-based liquid junction solar cells, the integration of ZnSe either as a compact overlayer on CdSe absorber, i.e. a window layer, or as a substitutional compound, upgrades the properties of the diode. For instance, the introduction of Zn in the CdSe lattice increases the energetic gap leading to higher open circuit potentials, thus higher efficiencies (even with a doping amount in the order of 1%) as well as enhanced stability [14]. Therefore, the investigation of the ZnSe-doping in CdSe is intended to the fabrication of optically graded devices, especially for photoelectrochemical solar cell applications.

Thermal, hot wall and electron beam evaporation, close space vapor transport and sintering were applied for the preparation of CdSe, ZnSe and ZCS thin films, to mention only a few methods. Besides, the soft growth techniques such as solution-growth or electrodeposition present a great interest, provided that the specifications of the products allow polycrystallinity. An electrochemically fabricated, band-gap engineered system of cadmium–zinc-selenide was originally reported [6], being in particular, a composition-modulated ''superstructure'' resulting from the application of electrodeposition cycles. Microcrystalline films prepared by electrochemical reduction of the precursor species on conducting substrates were reported in a few works [7, 14]. When applied for ZCS, the typical electrocrystallization

M. Bouroushian (✉) · T. Kosanovic
General Chemistry Laboratory, School of Chemical Engineering, National Technical University of Athens, Zografos Campus, 157 80 Athens, Greece
E-mail: mirtatb@central.ntua.gr
Tel.: +30-210-7723097
Fax: +30-210-7723088

process involves the underpotential reduction of at least one of the metal-ion species (the less noble zinc) from acidic solutions. However, the direct formation of the alloy is not plain, basically due to the difference in the redox potentials of Zn^{2+} and Cd^{2+} ions. Hitherto, the products of simple electrodeposition are not applicable, if well-defined compact films of solid solution are to be formed. A suitable post treatment (e.g. annealing) is usually used after deposition in order to improve the properties but the advantages of a single step method of preparation are thus lost. In any case, the multiple-gap electrodeposited thin films (either CdSe/ZnSe or ZCS) have a great potential for improved photoelectroconvertibility, and electrocrystallization offers the well-known advantages of low cost, large area deposition and versatile control.

A brief report on the typical electrodeposition method is presented here, focusing mainly in the compositional character of the obtained layers in terms of the atomic and phase composition.

Materials and methods

The electrochemical investigation of the ZCS system and the cathodic electro-crystallization of the selenide compounds took place in aqueous, acidic (pH = 2–4) baths of selenite (SeO_2) and metal-sulphate precursors. The $ZnSO_4$ concentration was kept constant at 0.2 M while varying the contents of the other constituents: $[Se^{(IV)}] = 0.5 - 2\times10^{-3}$ M and $[Cd^{2+}] = 0.1 - 20\times10^{-3}$ M. The bath-pH was adjusted by sulfuric acid at the working temperatures. The electroplating was performed in a potentiostatic mode at a temperature of 85 °C in a three-electrode cell fitted to a potentio-scan system (Wenking PGS 81R). Titanium and nickel discs ($\approx$1.13 cm^2) of commercial purity, abraded by sandpaper and polished by 0.25 μm alumina powder, were used as working electrodes. The Ti surface was further etched by 10% HF for 10 s in order to remove the superficial oxide layer. The counter electrode was a platinum grid and the reference electrode was a commercial Hg/Hg_2SO_4 saturated sulphate cell (SSE), which the potentials in this text refer to (there was no correction for ohmic drop). A rotating disc electrode setup with a 500-rpm angular speed was arranged to control the mass transfer in the bath.

Polycrystalline $Zn_xCd_{1-x}Se$ samples with $x = 0.2$, 0.4, 0.5, 0.6, 0.7 and 0.8 were also prepared by sintering of the constituent compounds. That is, commercial CdSe and ZnSe powders of high purity were blended at various molar ratios and cast to pellets under pressure. The raw pellets were sintered in an argon atmosphere under 800 °C for 1 h. The heating procedure was experimentally specified to give reliable results in terms of structure. The crystalline structure of the deposits and pellets was determined by X-ray diffraction (XRD) with a Siemens D5000 XRD with a CuKα source. Compositional data were obtained by energy-dispersive X-ray (EDX) analysis in a JEOL JSM 6100 apparatus.

Results and discussion

Voltammetry and deposition

The co-reduction of Se(IV), Cd(II) and Zn(II) species in an acidic environment under appropriate kinetic conditions may result in the formation of $Zn_xCd_{1-x}Se$ crystallites, via a simplified reduction scheme (Eq. 1, 2) formulated earlier [15, 16] to explain the electrodeposition of stoichiometric binary selenides.

$$Se^{(+IV)}O_2 \cdot H_2O + 4e^- + 4H^+ \rightarrow Se^{(0)}(ads) + 3H_2O \quad (1)$$

$$M^{2+}(ads) + Se(ads) + 2e^- \rightarrow MSe(s) \quad (2a)$$

$$xZnSe(s) + (1-x)CdSe(s) \rightarrow Zn_xCd_{1-x}Se \quad (2b)$$

where M ≙ metal. In a binary precursor bath, the selenium adatoms are thought to combine with the (more oxidizable) ad-ions of Cd^{2+} or Zn^{2+} and trigger their *underpotential* discharge through the negative-free energy increment of the compounds' formation (Eq. 2a). However, when depositing from a mixed solution, the cadmium ions are reduced *overpotentially* in the major part of experimental conditions, since highly cathodic potentials are required to approach the redox value of the less noble zinc. As also, a large amount of the $Se^{(+IV)}$ species undergoes a $6e^-$ per particle reduction (Eq. 3) [15], the electrogenerated Se^{-2} (in a protonated form) may directly combine in the liquid media with the metal ions present, forming slightly soluble selenides [17]. The latter might precipitate on the cathodic surface (Eq. 4) or be swept into the electrolyte and lost for the solid phase, thus decreasing the efficiency of the process.

$$SeO_2 \cdot H_2O + 6e^- + 6H^+ \leftrightarrow H_2Se^{(-II)}(aq) + 3H_2O \quad (3)$$

$$xZn^{2+} + (1-x)Cd^{2+} + Se^{-2} \rightarrow Zn_xCd_{1-x}Se(s) \quad (4)$$

In addition, the homogeneously formed hydride from Eq. 3—and its dissociation products—reacts rapidly with $Se^{(+IV)}$ in the acidic environment yielding chemical $Se^{(0)}$, which forms colloidal species in the vicinity of the electrode [18]. This conproportionation of selenium may constitute a source for excessive Se in the electrodeposit, precipitating an elemental crystalline phase.

The range of electrochemical potentials within which the compounds and alloys can be formed was determined from the electric current–voltage characteristics of HF-acid-treated Ti and Ni RDE at acidic baths of various compositions. The voltammograms recorded in solutions of pH = 2 and 3, are shown in Fig. 1 for the Ti cathode (potential range: −0.6 to −1.6 V). In the absence of Cd^{2+} and Zn^{2+} species, the current at potentials more cathodic than about −0.7 V is basically due to $Se^{(0)}$ and $Se^{(-2)}$ formation, according to the Eqs. 1 and 3,

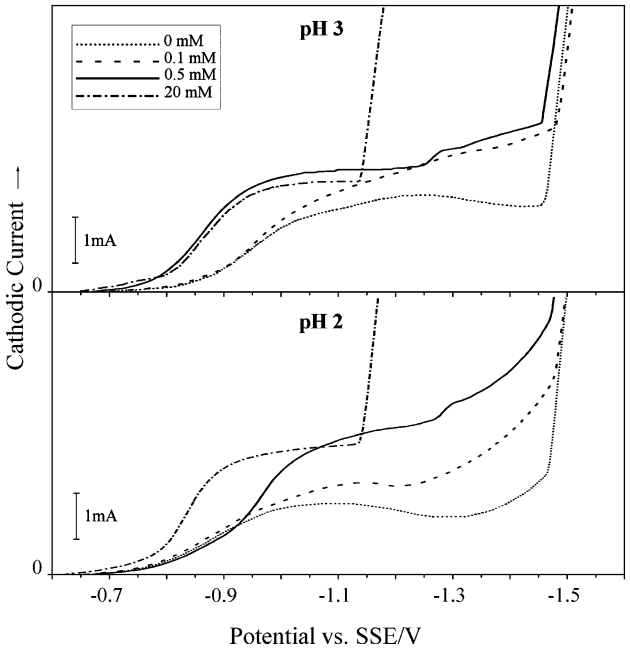

Fig. 1 Forward polarization sweeps on Ti RDE (500 rpm) at a rate of 5 mV/s in a bath 0.5×10^{-3} M in SeO_2, 0.2 M in $ZnSO_4$, pH = 2 and 3 and various concentrations ($0–20\times10^{-3}$ M) of $CdSO_4$ at 85 °C

superimposed by the electrochemistry of oxygen and hydrogen [16]. The presence of Zn^{2+} in the solution imposes a cathodic limit at its redox potential (about −1.45 V; Fig. 1). Addition of the nobler Cd^{2+} may give rise to a second reduction wave whose position and shape depends on the concentration. Between the Cd and Zn redox waves, and for low $[Cd^{2+}]$, a kinetically controlled domain may be established if a proper rotation of the working electrode (about 500 rpm) is applied. In this nearly potential-independent region, the electrolysis current is limited principally by the diffusion of Se and Cd ions towards the cathode, both finally discharging overpotentially. This situation is adjusted by maintaining an excess of Zn^{2+} ions, which suppresses the fast mass-transfer that would have occurred within the relevant potential range in zinc-free solutions, simply through the competition for cathodic adsorption sites. The mechanisms behind the dependence of current on potential are explicable in terms of the competition between the formation of CdSe and ZnSe, allowing also for the side effects involving the conproportionation of Se. More details on this complicated electrochemistry can be found at [15–18]. The side reactions associated with hydrogen become more important at lower pH and more negative potentials; however, the low pH (in combination with high temperature) promotes the formation of crystalline Se, which reacts on the surface cathode to produce CdSe–ZnSe. The employed pH of the bath then reflects a compromise between the undesired reactions diminishing the efficiency and the need to produce non-amorphous Se to trigger off the compound formation.

The electrolytic conditions were optimized in terms of composition, crystallinity and coherency of the films. In the following, the intensity and width of the (111) XRD reflection is taken as a rough measure of crystallinity, since the predominant structure of the obtained chalcogenide deposits is zinc-blend. The XRD intensity is normalized to charge per area, assuming a similar faradaic efficiency for the various samples; this is only an approximation as the mechanism is modified under different conditions of plating, so the resulting layers have different structures, densities and compositions. However, the shape and position of the diffraction peaks are thought to be sufficiently representative for our purposes.

Within the underpotential domain of cadmium, the Cd^{2+} ions neighboring the cathode produce a functional autoregulation effect consisting in their adsorption and subsequent reduction together with $Se^{(IV)}$ carriers. This gives rise to practically stoichiometric deposits of polycrystalline, (111) oriented cubic-blend CdSe. Departing from this potential region towards more cathodic potentials, from about −1.2 onwards, leads to a progressively larger doping amount of zinc and the texture is lost. Already at −1.2 V, the main *fcc* lines lie in between the values of the end member compounds, as shown in the XRD pattern in Fig. 2 (also Fig. 4), therefore they can be ascribed to the major existence of a cubic-blend ZCS phase.

Series of samples were produced from baths with various concentrations. A phase of CdSe contaminated by Zn, rather than a ternary alloy is formed from baths with high $[Cd^{2+}]$/[Se(IV)] ratios. Also, sharp diffraction

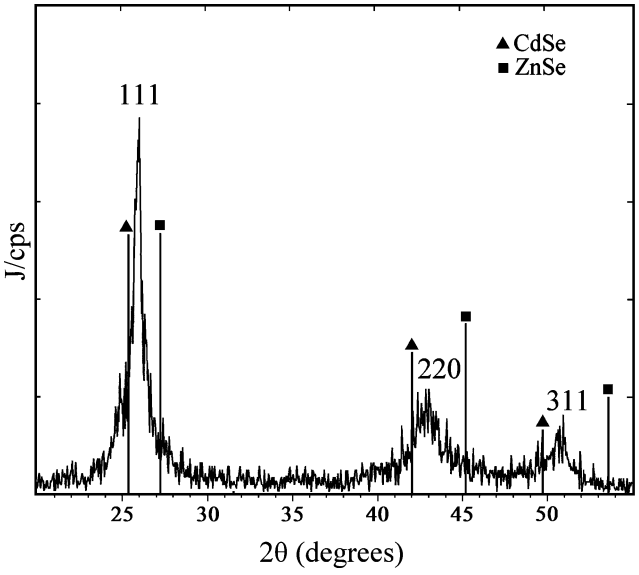

Fig. 2 X-ray diffractogram of a deposit prepared on HF-acid-treated Ti at −1.2 V from a 0.5×10^{-3} M SeO_2, 0.5×10^{-3} M $CdSO_4$, 0.2 M $ZnSO_4$, pH = 2 bath at 85 °C. The reflections of a ZCS zinc-blend structure are observed in between the respective lines of the end member compounds (CdSe and ZnSe of zinc-blend structure)

lines of metallic Cd throughout its overpotential region of deposition emerge, as shown in Fig. 3.

On the other hand, a quite low if not vanishing [Cd^{2+}] (=0.1 mM) and relatively high [Se(IV)] leads to the occurrence of a hexagonal Se phase together with CdSe in its hexagonal and cubic forms, as well as ZnSe. In general, at [Cd^{2+}]/[Se(IV)] < 1 there is a separation of phases in the solid deposits evidenced by distinguished sharp XRD lines of Se, CdSe, and ZnSe. In total, the electrodepositions performed by contemporaneously varying [Se(IV)] and [Cd^{2+}] under a constant excess of [Zn^{2+}], showed that equal Cd/Se concentrations operate more efficiently, as almost no excess phases of the constituents were detected. At any rate, the formation of a metallic Cd phase cannot be totally avoided since the process is deliberately ran at the overpotential region of the element (Fig. 4: −1.3 to −1.5 V), Therefore, [Cd^{2+}] is kept as low as possible in order to enable the ternary formation (commonly, 0.5 mM).

The increase of the negative deposition potential shifts the (100), (220) and (311) diffractions towards larger angles (i.e. the values of ZnSe), therefore signifying the formation of a ternary constituent (Fig. 4); however, this evolution is associated with a degeneration of the obtained films due to increased nucleation and chaotic growth. The disorder is partly due to the occurrence of a Cd phase, while also domains of pure Cd–Se bonding are grown together with the ZCS crystallites. The CdSe phase is manifested by the small shoulders before the main (111) feature in most XRD patterns, but a detailed treatment is needed to valuate its occurrence (see Composition analysis).

Composition analysis

Experimental *d*-values from XRD and quantitative elemental analysis from EDX were used in order to estimate the mole fraction (*x*) of the electroformed ZCS crystallites and the phase composition of the electro-deposits.

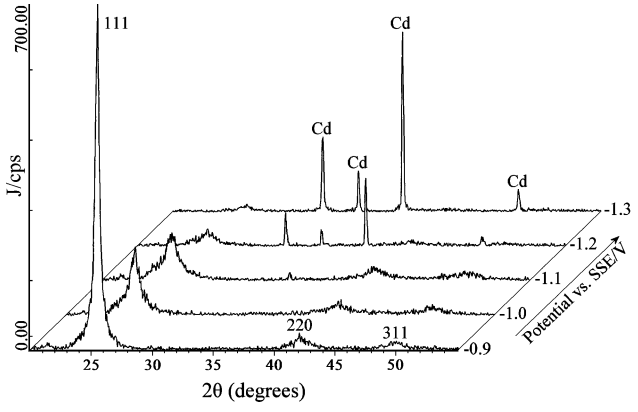

Fig. 3 XRD patterns of electrodeposits on HF-acid-treated Ti, obtained at increasingly cathodic potentials from a 0.5×10^{-3} M SeO_2, 0.02 M $CdSO_4$, 0.2 M $ZnSO_4$, pH = 3 bath at 85 °C

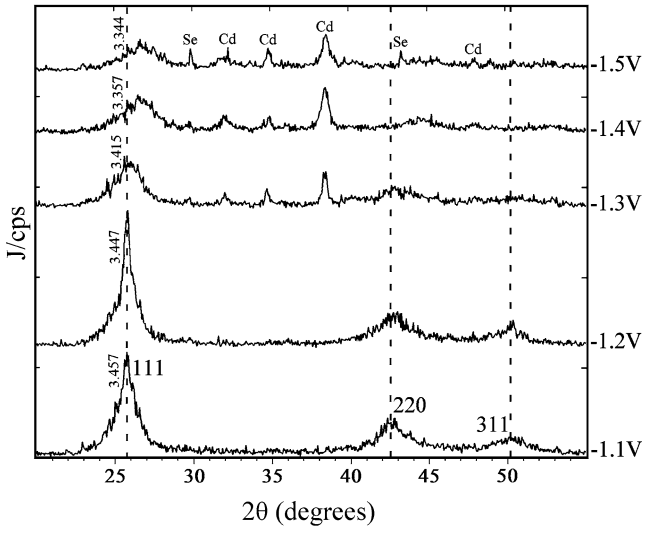

Fig. 4 XRD patterns of deposits grown on HF-acid-treated Ti at increasingly cathodic potentials from a 0.5×10^{-3} M SeO_2, 0.5×10^{-3} M $CdSO_4$, 0.2 M $ZnSO_4$, pH = 3 bath at 85 °C. The *arithmetic values* indicate the average *d*-spacing values (in Å) for the (111)/(00.2) reflections, while the *dashed lines* represent reference positions measured from the deposit obtained at −1.1 V

A first approximation was made on the basis of the straightforward scheme of Vegard's rule (Eq. 5a) with respect to a constant crystal structure; assuming a pure zinc-blend symmetry throughout the composition range—since this is presumably the predominant type of structure—and allowing for the *d*-spacing of the (111) cubic planes to substitute for the *a* dimension of the unit cell ($d_{111} = a\sqrt{3}$) we assign *x*-values to each electrodeposit via Eq. 5b by careful profile averaging of the (111) XRD peak positions to get precise d_{111}-values.

$$a = x \cdot a_{ZnSe} + (1 - x) \cdot a_{CdSe} \quad (5a)$$

$$d_{111} = x \cdot d_{111}(ZnSe) + (1 - x) \cdot d_{111}(CdSe) \quad (5b)$$

However, the accuracy of the linear law is questionable. *Moreover*, CdSe and ZnSe can be found in both cubic–zinc-blend (ZB) and hexagonal wurtzite (W) structures, while bulk $Zn_xCd_{1-x}Se$ is known to crystallize either in ZB for $x > 0.7$ or in W structure for $x < 0.5$, or in a mixture of both for $0.5 \le x \le 0.7$—since ZnSe is mostly obtained as ZB [2, 4, 9]. Most XRD patterns are not clearly resolved, so these phases may occur in the electrodeposited layers whose disorder is obvious. In order to allow for these complications, *sintered* pellets of defined composition were synthesized, to be used as reference phases. The diffraction patterns obtained for a series of sintered samples confirmed the formation of polycrystalline $Zn_xCd_{1-x}Se$ as shown in Fig. 5. Since no additional phases were identified, it is considered that the reaction between the selenide compounds gave alloy phases of narrow stoichiometry. It is worth noting that the intermediate compositions ($0.4 < x < 0.7$) of ZCS are associated to a certain disturbance of the lattice owing to the different sizes of substitution metals; in general, the

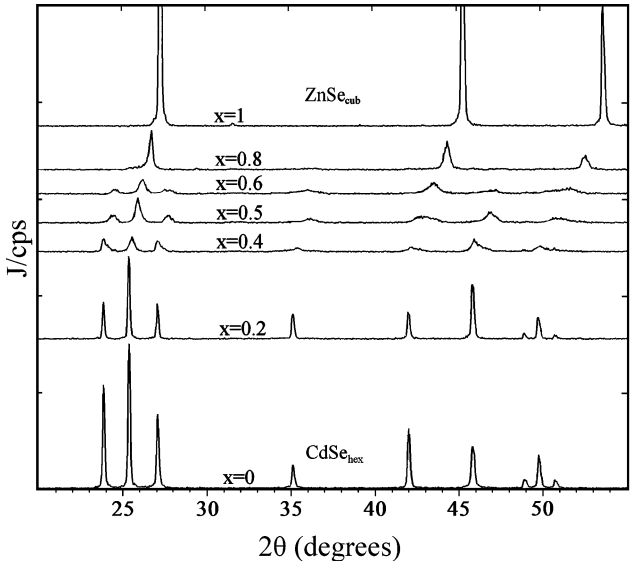

Fig. 5 XRD patterns of $Zn_xCd_{1-x}Se$ pellets for a series of mole fractions (x) used as external standards. The *upper* and *lower diagrams* correspond to the pure end-members

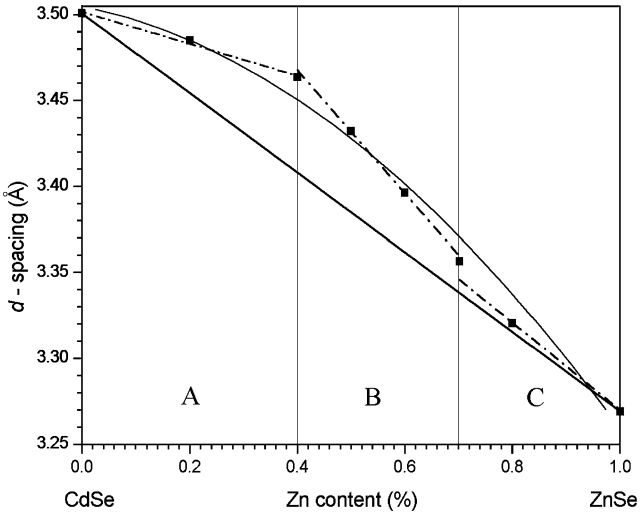

Fig. 6 Continuous variation of interplanar d-spacing of $Zn_xCd_{1-x}Se$ throughout the range of compositions versus the mole fraction of Zn, expressed by (1) the Vegard's law (*straight line*), (2) polynomial and sectional fittings of reference points (*black cubes*) measured from sintered pellets of known composition. The segments at the A, B, C regions correspond to different structures (*A* wurtzite, *B* mixed wurtzite and zinc-blend, *C* zinc-blend)

insertion of zinc results in shrinkage of the CdSe lattice—due to the smaller radius of Zn^{2+} (0.074 nm) with respect to Cd^{2+} (0.081 nm)—and this change has consequences on the lattice perfection of the substitutional solid solution. Note though, that a *swelling* of CdSe lattice due to the incorporation of Zn in *interstitial* positions, and/or the Se excess was also reported [14].

Reference points were defined by using $d_{00.2}$ values from the pellets' patterns within the region of "hexagonal" compositions, and $d_{111/00.2}$ values within the "intermediate region", thus specifying domains of uniform structure (Fig. 6). This was feasible because in the low and intermediate x-regions, the close packed (111) cubic planes transform into the close packed (00.2) hexagonal ones; considering the consequent change of the shape and size of the cubic cell, i.e. from a-parameter to c with respect to the specific axis, the d-spacing of (00.2) planes ($d_{00.2} = c/2$) can be used instead of the (111)-spacing. The experimental points within each structure domain were found to vary almost linearly with mole fraction, although the slopes were no longer the same with the Vegard's line, except for the ZB points in the C-region.

Thus, reference lines were drawn in order to perform interpolations (Fig. 6). Also, in order to account for the limited number of standards, a polynomial fit of all the experimental d-spacings from the pellets was used as an additional curve for interpolation. It is important to point out that these standards introduced a correction for structure but not for the deviations from linearity, since no ZB standards could be used for $0 < x < 0.7$. The only evidence is for $x > 0.7$ where, in effect, the experimental measurements were in close agreement with Vegard's prediction.

The above-mentioned approach assigns different x-values for each experimental d-spacing measurement from the electrodeposits. Taking their average, we calculate the XRD-related mole fractions, $x_{(XRD)}$, with respect to the preparation conditions. These are expected to denote the composition of a uniform ZCS phase independently of the possible presence of other phases. Some representative results are depicted in Fig. 7 for specific preparation conditions.

It is observed that the ZnSe fraction increases with the cathodic potential of deposition as expected. The rise

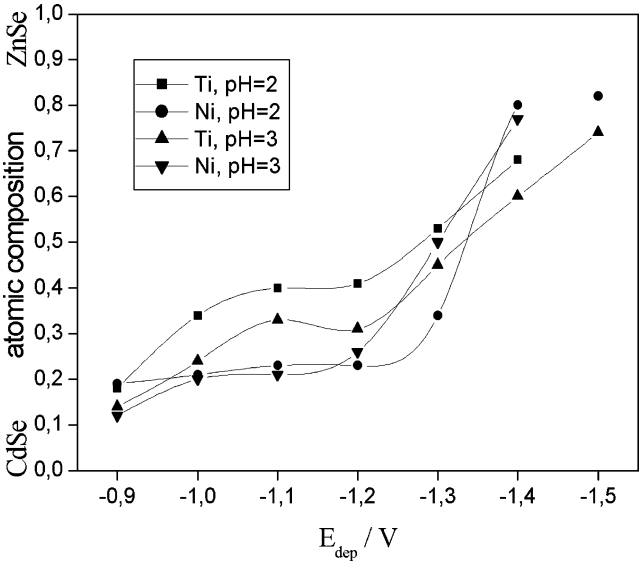

Fig. 7 The atomic composition (mole fraction) of the ternary phases formed by electrodeposition as a function of deposition potential, for the indicated cathode substrates and bath pH-values. The composition of the bath is as in Figs. 2 and 4

of the population of zinc atoms bound in the solid lattice is accompanied with the increase in the deposition current (Fig. 1), so that the co-deposition mechanism may be strongly determined by the adsorption and reduction of Zn^{2+} ions. It is worth noting that a non-zero fraction of Zn is obtained even in the underpotential region of Cd, i.e. in the range −0.9 to −1.1 V, especially on Ti (Fig. 1, 7); the attainable x-value reaches $x = 0.4$ with Ti cathodes and low pH, while a maximum of $x = 0.2$ is found with Ni substrates. This effect is due to the strong reaction of zinc with selenium, even deeply within the underpotential domain for Zn, through either or both the mechanisms previously discussed, and ensures that a high level of doping can be achieved at the relevant potentials. The films are compact and well crystallized, since no metallic Cd is formed within this range and the nucleation rate is low. In total, according to measurements in repeated depositions, results like those in Fig. 7 were characterized by a maximum deviation in the order of ± 0.05 and usually not larger than ± 0.02 for x. Therefore, the reproducibility is satisfactory.

The proportion of the different phases occurring in an electrodeposit can be determined with the aid of EDX data. According to XRD, and the underpotential nature of Zn^{2+} reduction, it is reasonable to assume that the totality of zinc atoms belongs to the lattice of a *ternary phase*, i.e. that there exists no pure ZnSe or Zn phases. Then, having an elemental analysis in hand, in terms of atom or mass percent averaged on the entire surface of a deposit, the mole fraction x is straightforward, and also the excess phases are identified after assigning the equivalent quantities of Se and Cd to the ternary phase. However, the $x_{(EDX)}$-values calculated in this manner are frequently smaller than $x_{(XRD)}$ (Table 1).

Considering the $x_{(XRD)}$ as the "true" value imposes a limiting condition, namely that an amount of CdSe should be removed from ZCS. Then a discrete CdSe phase exists in the layer (although this is not clear from the XRD patterns). Since there is also diffraction from Cd, an excess of metallic Cd exists as well. The numerical treatment of EDX data, taken in the form of the mass contents of the Zn, Cd and Se species, involves the solution of a system of mass balance equations for each element, assuming the occurrence of the above-mentioned phases (ZCS, CdSe, Cd). Thus, for an example, a sample with 3.30 Wt.% Zn, 41.4 Wt.% Se and 55.3 Wt.% Cd known to contain a $Zn_{0.26}Cd_{0.74}Se$ phase is found to consist of 34.8 Wt.% $Zn_{0.26}Cd_{0.74}Se$, 63.2 Wt.% CdSe and 2.0 Wt.% Cd. Some results of these calculations are given in Table 1.

Table 1 Atomic composition of electrogrown $Zn_xCd_{1-x}Se$ as estimated from XRD [$x_{(XRD)}$] and EDX [$x_{(EDX)}$], and mass percentage of the distinguished phases occurring in the deposits, prepared at the shown potential E_{dep} and substrate. CdSe and Cd percentage was calculated as described in text

E_{dep}/substrate	$x_{(XRD)}$	$x_{(EDX)}$	CdSe (Wt.%)	Cd (Wt.%)
−1.1 V/Ni	0.23	0.11	53.0	2.2
−1.4 V/Ni	0.82	0.68	23.2	22.4
−1.1 V/Ti	0.32	0.11	65.4	2.0
−1.3 V/Ti	0.49	0.32	31.1	25.7

It is generally estimated that a high proportion of CdSe (about 60%) exists at layers, which are deposited at potentials preceding the redox value of Cd. As the potential exceeds more and more the crystallization overpotential, so the rate of nucleation is increased, the layers become increasingly microcrystalline and both Cd and CdSe phases together with Zn-rich ZCS occur. In these conditions, the sum of the mass proportions of CdSe and Cd phases is around 40–50%. The disordered Zn-rich deposits consist of heterogeneous aggregates of crystallites, as confirmed by scanning electron microscopy (not presented here). The electrodeposition method is therefore endowed with a serious drawback, since a CdSe–Cd matrix is always present in a deposit. Thus, the single step growth is not able to provide ready-to-develop films, and a suitable post treatment is needed in order to obtain homogeneous and functional films.

The question that arises is whether the distribution of the zinc atoms is homogeneous, i.e. the degree of separation of the presumed distinct phases is to be determined. It is reasonable to assume that the existence of an individual CdSe phase is fallacious, since the response of CdSe vanishes in the background of the main XRD spectra features. Then the deposited films consist rather of ZCS crystallites of a wide composition range than well-resolved phases of narrow stoichiometry. It is worth noting that even if this is the case, the thermal annealing of the electrodeposits results in a recrystallization and separation of phases; according to preliminary experiments, the diffraction patterns obtained from post-deposition treated samples (heated for 1 h at 500 °C) give clear-cut diffraction lines, whose profiling reveals that a ternary constituent exists with a mole fraction quite close to that estimated by the previous analysis. In principle, this result supports the present method for determining the composition; however, even if well-defined phases are resolved, the admixtures exist and the technical problem is simply transposed. In any case, a thorough investigation on annealed deposits is needed to reach final conclusions.

Conclusions

Polycrystalline thin films containing $Zn_xCd_{1-x}Se$ with a molar fraction $0.1 < x < 0.9$ were electrochemically obtained, from an aqueous acidic bath with low concentration in SeO_2 and $CdSO_4$ and a working excess of $ZnSO_4$, on RDE metallic cathodes under mass transfer control. The composition of the as-grown $Zn_xCd_{1-x}Se$ crystallites was estimated by XRD using a series of reference $Zn_xCd_{1-x}Se$ solid solutions of varying stoichiometry obtained by solid state synthesis. The obtained results in combination with EDX data allowed the determination of the *phase* composition of the

produced layers. According to this method, the electrodeposits typically consist of a mixture of CdSe, Cd and $Zn_xCd_{1-x}Se$, the composition depending strongly on the deposition potential.

With the above procedure, it is possible to predetermine the composition of the deposits by appropriately choosing the preparation conditions. An increasing with the cathodic potential Zn-content in the solid can be achieved; however, the question about the arrangement of the zinc atoms in the solid layer remains to be solved.

References

1. Brafman O (1972) Solid State Commun 11:447
2. Gupta P, Maiti B, Maity AB, Chaundhuri S, Pal AK (1995) Thin Solid Films 260:75
3. Alonso RG, Suh EK, Ramdas AK, Samarth N, Luo H, Furdyna JK (1989) Phys Rev B 40/6:3720
4. Sharma KC, Garg JC (1990) J Phys D Appl Phys 23:1411
5. Avendaño-López J, Castillo-Alvarado FL, Escamilla-Esquivel A, Contreras-Puente G, Oriz-López J, Zelaya-Angel O (1996) Solid State Commun 100(1):33
6. Krishnan V, Ham D, Mishra KK, Rajeshwar KJ (1992) J Electrochem Soc 139(1):23
7. Natarajan C, Nogami G, Sharon M (1995) Thin Solid Films 261:44
8. Husain M, Singh BP, Kumar S, Sharma TP, Sebastian PJ (2003) Sol Energ Mat Sol C 76(3):399
9. Ammar AH (2001) Physica B 296:312
10. Schock HW (1996) Appl Surf Sci 92:606
11. Gruszecki T, Holmström B (1993) Sol Energ Mat Sol C 31:227
12. Lakshmikumar ST, Rastogi AC (1995) Thin Solid Films 259:150
13. Natarajan C, Sharon M, Lévy-Clément C, Neumann-Spallart M (1994) Thin Solid Films 237:118
14. Darkowski A, Grabowski A (1991) Sol Energ Mat Sol C 23:75
15. Bouroushian M, Kosanovic T, Loizos Z, Spyrellis N (2000) Electrochem Commun 2:281
16. Bouroushian M, Kosanovic T, Loizos Z, Spyrellis N (2002) J Solid State Electrochem 6:272
17. Zuman P, Somer G (2000) Talanta 51:645
18. Alanyalioglu M, Demir U, Shannon C (2004) J Electroanal Chem 561:21